A Monte Carlo Based Response Matrix Method for Pin-wise Transport Calculations

Sori Jeon, Namjae Choi, Han Gyu Joo[*]
Department of Nuclear Engineering, Seoul National University,
1 Gwanak-ro, Gwanak-gu, Seoul, 08826 Korea
[*]*Corresponding author: joohan@snu.ac.kr*

1. Introduction

The response matrix method (RMM) is a famous two-step calculation method which would enable fast core transport calculation based on pre-generated response matrices. Due to its advantage that no homogenization is necessary, it once had stood as a compelling method for whole-core transport calculations. However, as the deterministic transport methods such as the method of characteristics (MOC) have become relatively cheap to be directly applied to the core analyses while providing much higher flexibility, RMM had gradually fallen out of interest.

However, RMM may stand out again in the modern trend of computing processor technology development. As artificial intelligence (AI) and big data industries which require a tremendous amount of computing power are experiencing a significant growth, the processors are also being specialized to the operations used in those fields which involves large dense matrix operations. For example, a single GeForce RTX 2080 Ti GPU, which is consumer grade, is capable of delivering up to 110 TFLOPS of the matrix – matrix multiplication performance through the specialized tensor cores. It is equivalent to more than a thousand cores of typical server-grade CPU processors.

In this regard, we suggest an RMM formulation using the Monte Carlo (MC) method. The calculation of response matrices with MC was introduced in the direct response matrix (DRM) method of HITACHI [1] and the COMET code [2], and both works demonstrated promising results. In their works, however, the response matrices are fixed to an assembly configuration, which limits the flexibility. Therefore, we introduce a pin-wise RMM and examine its feasibility.

2. Response Matrix Method

To solve the neutron transport equation with RMM, four types of response matrices are defined for each pin type, which are generated by MC calculations. The response matrices should be obtained such that the computational costs be reduced via techniques such as Legendre polar angle expansion. The overall calculation scheme involving RMM is detailed below.

2.1 Definition and Generation of the Response Matrices

Response matrices are generated for each pin type by solving MC fixed source problems for the pin cell. The response matrices are classified into four types based on the neutron behaviors: transmission (surface-to-surface,

SS), escape (volume-to-surface, VS), neighbor-induced fission (surface-to-volume, SV), and self-induced fission (volume-to-volume, VV). The definitions of the response matrices, denoted as **R**, are as follows:

Transmission: $J_{out}^{\mu', \alpha', g', s'} = \mathbf{R}_{SS} J_{in}^{\mu, \alpha, g, s}$. (1)

Escape: $J_{out}^{\mu', \alpha', g', s'} = \mathbf{R}_{VS} \psi^{g, r}$. (2)

Neighbor-induced fission: $\psi^{g', r'} = \mathbf{R}_{SV} J_{in}^{\mu, \alpha, g, s}$. (3)

Self-induced fission: $\psi^{g', r'} = \mathbf{R}_{VV} \psi^{g, r}$. (4)

where J is the current vector and ψ is the fission source vector. Here, the current term retains angle-dependence; namely, it is characterized by the polar angle (μ) and the azimuthal angle (α) as well as the energy group (g) and the surface (s). Fission source has group and region (r) dependence and is considered isotropic. From now on, the phase space superscripts will be omitted for brevity.

The transmission and escape matrices determine the outgoing responses of a pin; they represent the expected number of outgoing neutrons on a surface s' by a neutron incoming from a surface s or departed from a region r, respectively. On the contrary, neighbor- and self-induced fission matrices evaluate the internal responses of a pin; they describe the expected number of fission neutrons in the volume r' by a neutron coming from a surface s or volume r, respectively. **Figure 1** schematically illustrates the four types of responses considered by each response matrix.
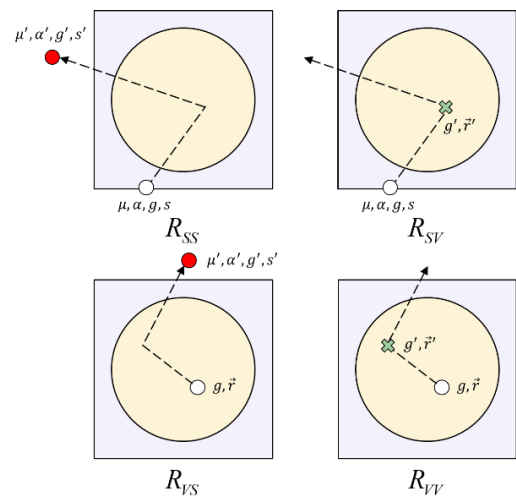
Figure 1. Illustration of the types of responses

The discretization parameters are fixed throughout this work, which were determined empirically to be optimal. 24 azimuthal angles and 16 polar angles are used in the

hemisphere on each surface; due to axial symmetry, only upper 12 azimuthal angles are considered. Each side of a pin is divided into three surfaces and the fuel consists of regions divided by three rings and four azimuthal sectors. **Figure 2** illustrates the discretization structure of a pin.
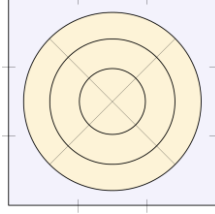
Figure 2. Discretization of a pin

The response matrix generation procedure with MC is as follows:

1. Depending on whether the response matrix to generate is current-induced or source-induced, the neutrons are uniformly created either on a surface (s) or in a region (r) with isotropic angle (μ, α) and random energy (g). The number of input neutrons created in each bin of phase space is scored at $I_S(\mu, \alpha, g, s)$ or $I_V(g, r)$.
2. Each neutron is simulated until it reaches a surface. Neutron weights are reduced by implicit capture but Russian roulette is not used.
3. If a neutron escapes a surface (s') with angle (μ', α') and energy (g'), its weight is scored:
$$\mathbf{R}_{SS} \leftarrow \mathbf{R}_{SS}(\mu, \alpha, g, s \to \mu', \alpha', g', s') + w, \quad (5)$$
$$\mathbf{R}_{VS} \leftarrow \mathbf{R}_{VS}(g, r \to \mu', \alpha', g', s') + w. \quad (6)$$
4. If a neutron undergoes a fission reaction in a region (r') and produces v neutrons with energy (g'), the yield is scored:
$$\mathbf{R}_{SV} \leftarrow \mathbf{R}_{SV}(\mu, \alpha, g, s \to g', r') + v, \quad (7)$$
$$\mathbf{R}_{VV} \leftarrow \mathbf{R}_{VV}(g, r \to g', r') + v. \quad (8)$$
5. Once all the neutrons are traced, the scored responses are divided by the input neutron scores to obtain unit responses, which becomes the response matrices:
$$\mathbf{R}_{SS} \leftarrow \mathbf{R}_{SS}(\mu, \alpha, g, s) / I_S(\mu, \alpha, g, s), \quad (9)$$
$$\mathbf{R}_{VS} \leftarrow \mathbf{R}_{VS}(g, r) / I_V(g, r), \quad (10)$$
$$\mathbf{R}_{SV} \leftarrow \mathbf{R}_{SV}(\mu, \alpha, g, s) / I_S(\mu, \alpha, g, s), \quad (11)$$
$$\mathbf{R}_{VV} \leftarrow \mathbf{R}_{VV}(g, r) / I_V(g, r). \quad (12)$$

2.2 Legendre Polar Angle Expansion

In RMM, most of the computing time is spent for the transmission calculation; namely, multiplication of $\mathbf{R}_{SS}$ and J_{in}. As can be easily inferred, $\mathbf{R}_{SS}$ is the largest matrix out of the four types of the response matrices. If all the variables are incorporated into the matrix in a discretized form, the dimension of the matrix easily reaches tens of thousands. This results in an impractical memory usage and computing time as the multiplication is repeatedly performed. Therefore, it is necessary to take a measure to reduce the size of the matrix.

In this regard, a polar angle expansion technique based on Shifted Legendre Polynomials (SLP) is introduced. It can reduce the number of polar angle components in the matrix from the number of polar angles to the number of moments which is determined by the expansion order. In principle, sufficient number of polar angles must be used for accuracy because it has large impact on the reactivity due to the self-shielding effect. However, it was observed that the distribution of current in μ shows fairly smooth behavior so that it can be adequately fitted by low-order polynomials. In this work, 2nd order expansion is chosen, and therefore only 3 coefficients are required to express the polar angle dependence of current as follows:

$$J(\mu) = \sum_{l=0}^{2} \tilde{J}^l P_l(\mu), \quad (13)$$

where P_l is the l-th order SLP and $\tilde{J}^l$ is the l-th moment.

In accordance with the expansion, we need to tally the polar angle moments of the outgoing neutrons. It can be achieved by the MC functional expansion tally technique. The orthogonality of SLP yields the following relation between the moment and the current:

$$\tilde{J}_{out}^l = (2l+1)\int_0^1 J_{out}(\mu)P_l(\mu)d\mu. \quad (14)$$

Thus, by simply scoring $(2l+1)P_l(\mu)$ for each outgoing neutron, the response in terms of moments can be tallied.

Resultantly, the transmission equation is reformulated as follows:

$$\tilde{J}_{out} = \tilde{\mathbf{R}}_{SS}\mathbf{P}\tilde{J}_{in}, \quad (15)$$

where $\tilde{\mathbf{R}}_{SS}$ is a modified transmission matrix that gives the moments as the response for the incoming currents, and $\mathbf{P}$ is a conversion matrix that calculates the physical currents from the moments, whose entries are merely the piece-wise integrals of the SLPs:

$$P_{ij} = \int_{\mu_{i-1}}^{\mu_i} P_j(\mu)d\mu. \quad (16)$$

In actual calculations, $\tilde{\mathbf{R}}_{SS}\mathbf{P}$, which is much smaller than the original transmission matrix $\mathbf{R}_{SS}$, is used as the single response matrix and the currents are carried in the moment form.

Note that the equations for the escape response and the neighbor-induced fission response should be modified as well:

$$\tilde{J}_{out} = \tilde{\mathbf{R}}_{VS}\psi, \quad (17)$$
$$\psi = \mathbf{R}_{SV}\mathbf{P}\tilde{J}_{in}. \quad (18)$$

In the same manner, $\mathbf{R}_{SV}\mathbf{P}$ is stored as a single response matrix.

2.3 CMFD Acceleration

As a fission source convergence acceleration scheme, CMFD acceleration is introduced to RMM. However, as RMM neither calculates flux nor employs cross sections which are necessary to calculate the homogenized group constants, response matrices for the flux and the reaction rates are also calculated by the procedure analogous to the primary response matrices.

The definition of the response matrices for the flux and the reaction rates are as follows:

$$x = \mathbf{R}_S^x \mathbf{P} \tilde{J}_{in} , \quad (19)$$

$$x = \mathbf{R}_V^x \psi . \quad (20)$$

where x is the desired quantity which is pin-homogenized, and $\mathbf{R}_S^x$, $\mathbf{R}_V^x$ are current- and source-induced response matrices of x, respectively.

Once the pin-homogenized flux and reaction rates are obtained throughout the RMM iteration, group constants can be calculated and CMFD acceleration can be carried out. The response matrices for the CMFD acceleration are small and does not add much computational overhead to the main RMM procedure.

2.4 Power Iteration Scheme

The algorithm for solving the k-eigenvalue problem with RMM is presented in **Figure 3**. First, the response contributions of the initial fission sources are calculated, namely [1] the escape response that gives initial currents on the surfaces and [2] the self-induced fission response. It is followed by the inner iteration which [3] iteratively updates the currents on the surfaces by the transmission response and [4] accumulates the fission sources for the next outer iteration step by the neighbor-induced fission response. Note that at each inner iteration step, every pin has to receive the outgoing currents of the adjacent pins and update its own incoming currents, which also adds a certain amount of overhead. Accumulation of the CMFD quantities is also done in appropriate locations.

The inner iteration is continued until the currents are fully attenuated. Once the inner iteration had converged, the remaining procedures are analogous to the ordinary power iteration incorporating CMFD acceleration.

OUTER : DO WHILE Not Converged

　[1] Escape: $\tilde{J}_{out} = \tilde{\mathbf{R}}_{VS} \psi_0$

　[2] Self-induced fission: $\psi = \mathbf{R}_{VV} \psi_0$

　Accumulate source-induced flux and reaction rates

　INNER : DO WHILE $\left\| \tilde{J}_{out}^0 \right\| > \varepsilon$

　　Update $\tilde{J}_{in}$ using $\tilde{J}_{out}$

　　[3] Transmission: $\tilde{J}_{out} = \tilde{\mathbf{R}}_{SS} \mathbf{P} \tilde{J}_{in}$

　　[4] Neighbor-induced fission: $\psi = \psi + \mathbf{R}_{SV} \mathbf{P} \tilde{J}_{in}$

　　Accumulate current-induced flux and reaction rates
　　Accumulate surface net currents

　END DO INNER

　Update eigenvalue

　Check convergence

　Perform CMFD acceleration and update ψ

　Save old fission source: $\psi_0 = \psi$

END DO OUTER

Figure 3. Power iteration algorithm

3. Results

In this section, accuracy and performance of RMM are evaluated by a comparative study with the MOC solver of nTRACER [3]. An MC code PRAGMA [4] is used as the reference. The problems are based on the C5G7MOX benchmark problem but manipulated in some degree to discover the distinction of RMM from the conventional MOC solver. The nTRACER calculations were carried out with 0.01cm ray spacing and 16/4 azimuthal/polar angles were used in octant.

3.1 Single Assembly Calculations

Here, five types of assemblies are examined whose configurations are shown in **Figure 4**. A1 and A2 are the ordinary UO_2 and MOX fuel assemblies of the benchmark, and I1 to I3 are the variations which contain highly concentrated absorbers that mimic the integrated fuel burnable absorber (IFBA). The IFBA-like absorbers were designed by coating the control rod material in the benchmark on the surface of the fuel rods with 0.001cm thickness. The absorption cross sections of the control rod material were then increased by 40 times.

IFBA is the typical weak point of MOC which suffers from the ray effects; as the IFBA regions are way much thinner than the 'beams' represented by the rays, reaction rates in the IFBA region are highly biased. On the other hand, RMM captures the MC physics and theoretically it can handle any problems that the MC method can solve.

Table 1 shows the eigenvalues of the assemblies and the errors of each method. The PRAGMA results were obtained using 10 billion histories. As expected, RMM reveals its strength in handling nonconventional problems that MOC cannot solve properly. A peculiar error in A2 of RMM still requires investigations. It is, however, clearly seen that the accuracy of RMM is not affected by the existence of IFBA while MOC shows large discrepancy. The error in I3 of RMM is caused by the baseline error of A2 and it is not due to IFBA itself.

□ UO2　□ MOX 4.3 %　□ MOX 7.0 %　■ MOX 8.7 %　■ UO2 + IFBA　■ MOX 8.7 % + IFBA
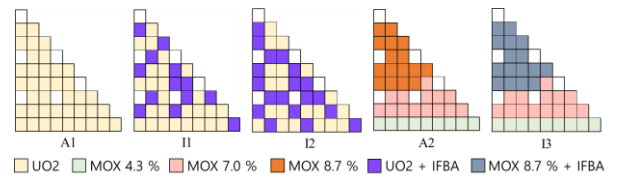
Figure 4. Configurations of the single assembly problems

Table 1. Eigenvalues of the single assembly problems

Case	PRAGMA	Δk_{eff} (pcm)	
		RMM	MOC
A1	1.33344 (1)	-13	17
A2	1.18565 (1)	-91	-1
I1	1.07529 (1)	-17	-203
I2	0.95271 (1)	-12	-272
I3	1.05076 (1)	-96	-111

3.2 2D Core Calculations

A fictitious core loaded with I1 and I3 assemblies was designed to verify the core analysis capability of RMM, as described in **Figure 5**. **Table 2** summarizes the results of eigenvalue and pin power errors, and the relative error distributions of pin powers are shown in **Figure 6.** Both codes used 10^{-5} convergence criteria for the relative norm of fission source change, and the MC reference solution was generated with 50 billion histories.

Although the two codes have comparable pin power RMS errors, RMM does not show any power tilt that is present in the MOC solution. In addition, RMM captures the transport effect better which occurs at the material interfaces such as fuel – moderator and UO_2 – MOX. The reactivity is also better estimated by RMM.
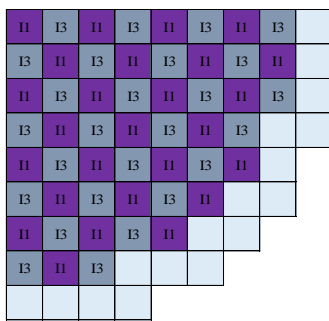
Figure 5. Configuration of the IFBA-bearing fictitious core

Table 2. Calculation results of the 2D core.

Case	k_{eff}	Δk_{eff} (pcm)	Max. Rel. ΔP (%)	RMS (%)
PRAGMA	1.05673	-	-	-
RMM	1.05626	-47	1.34	0.24
MOC	1.05522	-151	1.85	0.26
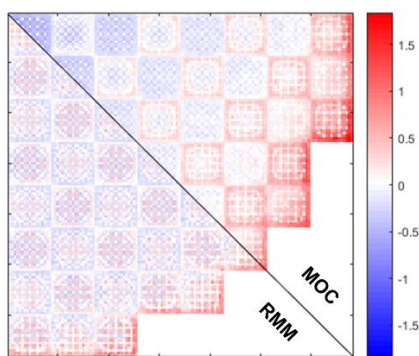
Figure 6. Relative error distributions of MOC and RMM

Nonetheless, the large computing time is the major drawback of RMM. **Table 3** compares the computing time of RMM and nTRACER, which were executed on 20 cores of Intel Xeon E5-2630 v4 CPUs. In RMM, calculation of $\mathbf{R}_{SS}$ and $\mathbf{R}_{SV}$, namely the inner iteration, contributes 75% and 20% to the total computing time, respectively, which leads to twice larger computing time

than nTRACER. It should be addressed to retain the feasibility of pin-wise RMM.

Table 3. Comparison of total computing time

Code	RMM	nTRACER
Computing Time (s)	2194.8	1031.4

4. Conclusions

An MC-based pin-wise response matrix method was introduced as a unique neutron transport solution scheme. The response matrices are generated for each pin type from fixed-source MC calculations. A polar angle expansion scheme using shifted Legendre polynomials was devised to reduce the computational cost and the CMFD acceleration was introduced in the response matrix framework.

Since the response matrices are calculated by an MC code, RMM can reflect all the MC physics inside a pin. This strength was clearly observed in the verification results for the fictitious IFBA-bearing assemblies made from the C5G7MOX benchmark problem. While MOC suffered from large reactivity errors due to the ray effect, RMM could accurately capture the effect of IFBA. Also for the IFBA-bearing fictitious core, RMM performed better than MOC; the power tilt was eliminated and the transports effect appearing at the material interfaces were better captured, as well as having lower reactivity error.

Still, substantive improvements are required for RMM. First of all, high computational cost has to be addressed by introducing more extensive expansions of variables. Especially, energy expansion is critical as expressing the continuous energy physics with the ordinary multi-group formulation will likely result in an impractical number of energy groups. In addition, problems with T/H feedback or depletion, in which the cross sections are continuously varied, should be considered.

REFERENCES

[1] M. Moriwaki, K. Ishii, H. Maruyama, M. Aoyama, "A New Direct Calculation Method of Response Matrices Using a Monte Carlo Calculation," Journal of Nuclear Science and Technology **36**(3), pp. 877-887 (1999).

[2] B. Forget, "A Three Dimensional Heterogeneous Coarse Mesh Transport Method for Reactor Calculations," Ph.D. Dissertation, Georgia Institute of Technology (2006).

[3] Y. S. Jung, C. B. Shim, C. H. Lim, H. G. Joo, "Practical Numerical Reactor Employing Direct Whole Core Neutron Transport and Subchannel Thermal/Hydraulics Solvers," Annals of Nuclear Energy **62**, pp. 357-374 (2013).

[4] N. Choi, K. M. Kim, H. G. Joo, "Initial Development of PRAGMA – A GPU-Based Continuous Energy Monte Carlo Code for Practical Applications" Proceedings of the Korean Nuclear Society Autumn Meeting, Goyang, Korea, Oct. 24-25 (2019).